

# A Sparse Non-negative Matrix Factorization Framework for Identifying Functional Units of Tongue Behavior from MRI

Jonghye Woo, *Member, IEEE*, Jerry L. Prince, *Fellow, IEEE*, Maureen Stone, Fangxu Xing, Arnold Gomez, Jordan R. Green, Christopher J. Hartnick, Thomas J. Brady, Timothy G. Reese, Van J. Wedeen, Georges El Fakhri, *Fellow, IEEE*

**Abstract**—Muscle coordination patterns of lingual behaviors are synergies generated by deforming local muscle groups in a variety of ways. Functional units are functional muscle groups of local structural elements within the tongue that compress, expand, and move in a cohesive and consistent manner. Identifying the functional units using tagged-Magnetic Resonance Imaging (MRI) sheds light on the mechanisms of normal and pathological muscle coordination patterns, yielding improvement in surgical planning, treatment, or rehabilitation procedures. Here, to mine this information, we propose a matrix factorization and probabilistic graphical model framework to produce building blocks and their associated weighting map using motion quantities extracted from tagged-MRI. Our tagged-MRI imaging and 4D (3D space with time) voxel-level tracking provide previously unavailable internal tongue motion patterns, thus revealing the inner workings of the tongue during speech or other lingual behaviors. We then employ spectral clustering on the weighting map to identify the cohesive regions defined by the tongue motion that may involve multiple or undocumented regions. To evaluate our method, we perform a series of experiments. We first use two-dimensional image and synthetic data to demonstrate the accuracy of our method. We then use three-dimensional synthetic and *in vivo* tongue motion data using protrusion and simple speech tasks to identify subject-specific and data-driven functional units of the tongue in localized regions.

**Index Terms**—Tongue Motion, Functional Units, Speech, Non-negative Matrix Factorization, MRI, Sparsity

## I. INTRODUCTION

Finding a suitable representation of high-dimensional and complex data for various tasks, such as clustering and topic modeling, is a fundamental challenge in many areas such as computer vision, machine learning, data mining, and medical image analysis. Non-negative matrix factorization (NMF) [1], an unsupervised generative model, is a class of techniques to identify a low-dimensional representation of a dataset suitable for a clustering interpretation [2]; it also has been used to transform different features to a common class. Since its introduction by Lee and Seung [1], special attention has been given

to NMF and its variants involving sparsity because of its ability to uncover a parts-based and interpretable representation based on physiological phenomena about the human brain [23]. Specifically, NMF with a sparsity constraint operates on input matrices whose entries are non-negative, thus allowing us to model a data matrix as sparse linear combinations of a set of basis vectors (or building blocks). In this work, we are interested in modeling the tongue’s underlying behaviors using NMF, since non-negative properties of NMF are akin to the physiology of the tongue as reflected in the matrix decomposition process. That is, NMF with a sparsity constraint only allows non-negative combinations of building blocks. This is analogous with the analysis of muscle synergies because a complex set of non-negative activations of tongue muscles generate the complexity and precision of the tongue’s voluntary and involuntary movements.

The human tongue is one of the most structurally and functionally complex muscular structures in our body system, comprising orthogonally oriented and highly inter-digitated muscles. The human tongue is innervated by over 13,000 hypoglossal motoneurons [3], [4]. A complex set of neural activations of tongue muscles allows to deform localized regions of the tongue in this complex muscular array. Muscle coordination patterns of the tongue are synergies produced by deforming local muscle groups—i.e., *functional units* [6], [7]. Functional units can be seen as an intermediate structure, which links muscle activity to surface tongue geometry, and which also exhibits cohesive and consistent motion in the course of specific tasks. Therefore, determining functional units and understanding the mechanisms by which muscles coordinate to generate target movements can provide new insights into motor control strategy in normal, pathological, and adapted tongue movements after surgery or treatment. This will, in turn, leads to improvement in surgical planning, treatment, or rehabilitation procedures. However, to date, the mechanisms of the muscle coordination patterns and the relationship between tongue structure and function have remained poorly understood because of the greater complexity and variability of both muscular structures and their interactions.

Understanding the subject/task-specific tongue’s functional organization requires a map of the functional units of the tongue during the oromotor behaviors using medical imaging. In particular, recent advances in medical imaging and associated data analysis techniques permit the non-invasive imaging

Part of this work was presented at the MICCAI 2014 and Acoustical Society of America in 2017. Jonghye Woo, Fangxu Xing, Thomas J. Brady, Timothy R. Reese, Van J. Wedeen, and Georges El Fakhri are with Department of Radiology, Massachusetts General Hospital and Harvard Medical School. Maureen Stone is with the University of Maryland Dental School. Jordan R. Green is with MGH Institute of Health Professions. Christopher J. Hartnick is with Massachusetts Eye and Ear Infirmary and Harvard Medical School. Arnold Gomez and Jerry L. Prince are with Department of Electrical and Computer Engineering at Johns Hopkins University.  
E-mail: jwoo@mgh.harvard.edu

and visualization of tongue structure and function in a variety of ways. Magnetic resonance imaging (MRI) technologies have been widely used, demonstrating that a large number of tongue muscles undergo highly complex deformations during speech and other lingual behaviors. For example, the ability to image non-invasively using MRI has allowed to capture both surface motion of the tongue via cine- or real-time MRI [8], [9], [10] and internal tissue point motion of the tongue via tagged-MRI (tMRI) [5]. In addition, high-resolution MRI and diffusion MRI [25], [24] have allowed to image the muscular and fiber anatomy of the tongue, respectively. With advances in computational anatomy, a vocal tract atlas [11], [12], a representation of the tongue anatomy, has also been created and validated, which allows for investigating the relationship between tongue structure and function by providing a reference anatomical configuration to analyze similarities and variability of tongue motion.

This work is aimed at developing a computational approach for defining the subject/task-specific and data-driven functional units from tMRI and 4D (3D space with time) voxel-level tracking [13] by extending our previous approach [17]. In this work, we describe a refined algorithm including an advanced tracking method and graph-regularized sparse NMF (GS-NMF) to determine spatio-temporally varying functional units using protrusion and simple speech tasks and offer extensive validations on simulated tongue motion data. Since standard NMF formulation hinges on a Euclidean distance measure (i.e. Frobenius norm) or the Kullback-Leibler divergence, it fails to mine the intrinsic and manifold geometry of its data [23]. Our method, therefore, makes use of both sparse and manifold regularizations to identify a set of optimized and geometrically meaningful motion patterns by promoting the computation of distances on a manifold from observed tongue motion data. Our formulation assumes that the tongue motion features live in a manifold space within a sparse NMF framework, thereby finding a low-dimensional yet interpretable subspace of the motion features from tMRI.

We present an approach to discovering the functional units using a matrix factorization and probabilistic graphical model framework with the following main contributions:

- The most prominent contribution is to use voxel-level data-driven tMRI ( $1.875\text{mm} \times 1.875\text{mm} \times 1.875\text{mm}$ ) methods incorporating internal tissue points to obtain subject-specific functional units of how tongue muscles coordinate to generate target observed motion.
- This work applies a graph-regularized sparse NMF and probabilistic graphical model to the voxel-level motion data, allowing us to estimate the latent functional coherence, by learning simultaneously hidden building blocks and their associated weighting map from a set of motion features.
- Our tMRI imaging and 4D voxel-level tracking paradigm provide previously unavailable internal tongue motion patterns. The proposed approach is scalable to a variety of motion features derived from motion trajectories to characterize the coherent motion patterns. In this work, we consider the most representative features including displacements and angle from tMRI.

The remainder of this paper is organized as follows. We first review related work in Section II. Section III shows the proposed method to identify functional units. The experimental results are presented in Section IV. Section V presents a discussion, and Section VI concludes this paper.

## II. RELATED WORK

In this section, we review recent work on NMF for clustering and functional units research that are closely related to our work.

**NMF for Clustering.** A multitude of NMF-based methods for unsupervised data clustering have been proposed over the last decade across various domains, ranging from video analysis to medical image analysis. In particular, the idea of using  $L_1$  norm regularization (i.e., sparse NMF) for the purpose of clustering has been successfully employed [28]. The sparsity condition imposed on the weighting matrix (or coefficient matrix) indicates the clustering membership. For example, Shahnaz et al. [29] proposed an algorithm for document clustering based on NMF, where the method was used to obtain a low-rank approximation of a sparse matrix while preserving natural data property. Wang et al. [31] applied the NMF framework to gene-expression data to identify different cancer classes. Anderson et al. [32] presented an NMF-based clustering method to group differential changes in default mode subnetworks from multimodal data. In addition, Mo et al. [33] proposed a motion segmentation method using an NMF-based method. A key insight to use NMF for clustering purpose is that NMF is able to learn and discriminate localized traits of data with a better interpretation. Please refer to [19] for a detailed review on NMF for clustering purpose.

**Speech Production.** Research on determining functional units during speech has a long history (see e.g., Gick and Stavness [14] for a recent perspective). Determining functional units is considered as uncovering a “missing link” between speech movements primitives and cortical regions associated with speech production [14]. In the context of lingual coarticulation, functional units can be seen as “quasi-independent” motions [3]. A variety of different techniques have been used to tackle this problem. For instance, Stone et al. [15] showed that four mid-sagittal regions including anterior, dorsal, middle, and posterior functioned quasi-independently using ultrasound and microbeam data. Green and Wang attempted to characterize functionally independent articulators from microbeam data using covariance-based analysis [6]. More recently, Stone et al. [3] proposed an approach to determining functional segments using both ultrasound and tMRI. That work examined compression and expansion between the anterior and posterior part of the tongue and found that regions or muscles have functional segments influenced by phonemic constraints. Ramanarayanan et al. [16] proposed to use a convolutive NMF method to identify motion primitives of the tongue using electromagnetic articulography (EMA). Our work is inspired by the aforementioned approaches and far richer 4D tMRI based voxel-level tracking and the augmented NMF framework is used to determine functional units. In addition, unlike other previous approaches that largely rely on the tracking of

landmark points sparsely located on the fixed tongue surface such as the tip, blade, body, and dorsum, we aim to identify 3D cohesive functional units that involve multiple, and possibly undocumented and localized tongue regions.

### III. METHODOLOGY

#### A. Problem Statement

Without loss of generality, let us first define the notations and definitions used in this work. Let us assume  $P$  internal points of the tongue derived from tMRI. We now define motion features at each voxel location, having  $n$  scalar quantities, such as magnitude and angle of each point track, precisely tracked through  $K$  time frames. Each tissue point is characterized by these scalar quantities, which are then used to cluster them into coherent motion patterns. We denote the position of the  $p$ -th tissue point at the  $l$ -th time frame as  $(x_l^p, y_l^p, z_l^p)$ . The tongue motion can be expressed as a  $3L \times P$  spatio-temporal feature matrix  $\mathbf{M} = [\mathbf{m}_1, \dots, \mathbf{m}_P] \in \mathbb{R}^{3L \times P}$ , where the  $p$ -th column is expressed as

$$\mathbf{m}_p = [x_1^p, \dots, x_L^p, y_1^p, \dots, y_L^p, z_1^p, \dots, z_L^p]^T. \quad (1)$$

The problem of identifying the functional units is viewed as a clustering problem, since the functional units are localized tongue regions that exhibit characteristic and homogeneous motions. However, different from generic motion clustering problems in computer vision or machine learning, the tongue's function and physiology also need to be reflected and captured in our formulation. Thus, we opt to identify a permutation of the columns to build  $[\mathbf{M}_1 | \mathbf{M}_2 | \dots | \mathbf{M}_c]$ , where the submatrix  $\mathbf{M}_i$  comprises tracks belonging to the  $i$ -th submotion, corresponding to the  $i$ -th functional unit. The motion quantities for each underlying muscle of the tongue are not completely independent. That is, our framework is data-driven and motion-specific at the sub-muscle level, which could be mapped from a subset of motion quantities from one or more muscles. These latent morphologies—i.e., functional units—inherent in higher dimensional datasets offer a sparse representation of the generative process behind the tongue's physiology for sub-muscle, a single or multiple muscles. To achieve this goal, the sparse NMF method is utilized to capture the latent morphologies from motion trajectories. The proposed method is described in more detail below; a flowchart is depicted in Figure 1.

#### B. MR Data Acquisition and Motion Tracking

1) *MR Data Acquisition:* All MRI data are acquired on a Siemens 3.0 T Tim Trio system with 12-channel head and 4-channel neck coil. While each participant performs the protrusion and simple speech tasks including “a geese” and “a souk” repeatedly in synchrony with metronome sound, the tMRI data are acquired using Magnitude Imaged CSPAMM Reconstructed images [26]. All tMRI data have 26 time frames with a temporal resolution of 36 ms with no delay during a 1 second duration. The resolution is  $1.875\text{mm} \times 1.875\text{mm} \times 6\text{mm}$ .

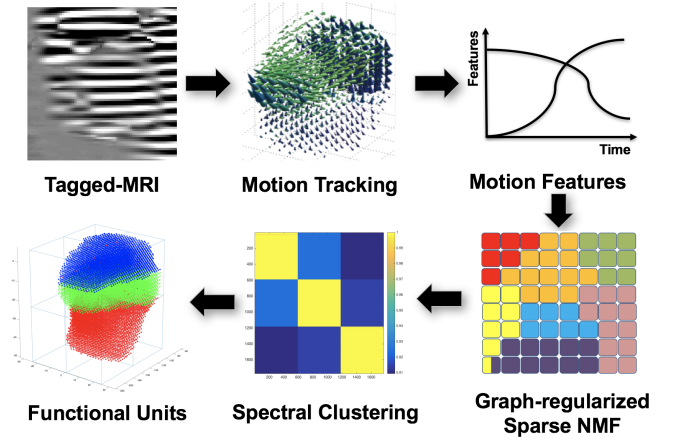


Fig. 1. Overview of the proposed method

#### 2) Voxel-Level Motion Tracking from Tagged-MRI:

The phase vector incompressible registration algorithm (PVIRA) [35] is used to estimate deformation of the tongue from tMRI, yielding a sequence of voxel-level motion fields. Although the input is a set of sparsely acquired tMRI slices, PVIRA uses cubic B-spline to interpolate these 2D slices into denser 3D voxel locations. Then a harmonic phase (HARP) [20] filter is applied to produce HARP phase volumes from the interpolated result. Finally, PVIRA uses the iLogDemons method [21] on these phase volumes. Specifically, we denote the phase volumes as  $\Phi_x, \Theta_x, \Phi_y, \Theta_y, \Phi_z,$  and  $\Theta_z$ , where  $x, y,$  and  $z$  denote motion information from three cardinal directions usually contained in orthogonal axial, sagittal, and coronal tagged slices. The volume in the reference time frame is  $\Phi$  and the volume in the deformed time frame is  $\Theta$ . The motion update vector field is derived from these phase volumes. At each voxel, the update vector is obtained by

$$\delta \mathbf{v}(\mathbf{x}) = \frac{\mathbf{v}_0(\mathbf{x})}{\alpha_1(\mathbf{x}) + \alpha_2(\mathbf{x})/S}, \quad (2)$$

Note that  $S$  is the normalization factor.  $\mathbf{v}_0(\mathbf{x})$ ,  $\alpha_1(\mathbf{x})$ , and  $\alpha_2(\mathbf{x})$  are defined by

$$\begin{aligned} \mathbf{v}_0(\mathbf{x}) &= W(\Phi_x(\mathbf{x}) - \Theta_x(\mathbf{x}))(\nabla^* \Phi_x(\mathbf{x}) + \nabla^* \Theta_x(\mathbf{x})) \\ &\quad + W(\Phi_y(\mathbf{x}) - \Theta_y(\mathbf{x}))(\nabla^* \Phi_y(\mathbf{x}) + \nabla^* \Theta_y(\mathbf{x})) \\ &\quad + W(\Phi_z(\mathbf{x}) - \Theta_z(\mathbf{x}))(\nabla^* \Phi_z(\mathbf{x}) + \nabla^* \Theta_z(\mathbf{x})), \\ \alpha_1(\mathbf{x}) &= \|\nabla^* \Phi_x(\mathbf{x}) + \nabla^* \Theta_x(\mathbf{x})\|^2 + \|\nabla^* \Phi_y(\mathbf{x}) + \nabla^* \Theta_y(\mathbf{x})\|^2 \\ &\quad + \|\nabla^* \Phi_z(\mathbf{x}) + \nabla^* \Theta_z(\mathbf{x})\|^2, \\ \alpha_2(\mathbf{x}) &= W(\Phi_x(\mathbf{x}) - \Theta_x(\mathbf{x}))^2 + W(\Phi_y(\mathbf{x}) - \Theta_y(\mathbf{x}))^2 \\ &\quad + W(\Phi_z(\mathbf{x}) - \Theta_z(\mathbf{x}))^2. \end{aligned} \quad (3)$$

Wrapping of phase  $W(\theta)$  is defined by

$$W(\theta) = \text{mod}(\theta + \pi, 2\pi) - \pi \quad (4)$$

and the “starred” gradient is defined by

$$\nabla^* \Phi(\mathbf{x}) := \begin{cases} \nabla \Phi(\mathbf{x}), & \text{if } |\nabla \Phi(\mathbf{x})| \leq |\nabla W(\Phi(\mathbf{x}) + \pi)| \\ \nabla W(\Phi(\mathbf{x}) + \pi), & \text{otherwise.} \end{cases} \quad (5)$$

After all iterations are complete, the forward and inverse deformation fields can be found by

$$\varphi(\mathbf{x}) = \exp(\mathbf{v}(\mathbf{x})) \text{ and } \varphi^{-1}(\mathbf{x}) = \exp(-\mathbf{v}(\mathbf{x})), \quad (6)$$

and they are both incompressible and diffeomorphic, making both Eulerian and Lagrangian computations available for the following continuum mechanics operations.

### C. Extraction of Motion Features

We first extract the motion features from PVIRA to characterize the coherent motion patterns. We use the magnitude and angle of each track as our motion features similar to [34] as described as

$$m_l^p = \sqrt{(x_{l+1}^p - x_l^p)^2 + (y_{l+1}^p - y_l^p)^2 + (z_{l+1}^p - z_l^p)^2} \quad (7)$$

$$oz_l^p = \frac{x_{l+1}^p - x_l^p}{\sqrt{(x_{l+1}^p - x_l^p)^2 + (y_{l+1}^p - y_l^p)^2}} + 1 \quad (8)$$

$$ox_l^p = \frac{y_{l+1}^p - y_l^p}{\sqrt{(y_{l+1}^p - y_l^p)^2 + (z_{l+1}^p - z_l^p)^2}} + 1 \quad (9)$$

$$oy_l^p = \frac{z_{l+1}^p - z_l^p}{\sqrt{(z_{l+1}^p - z_l^p)^2 + (x_{l+1}^p - x_l^p)^2}} + 1, \quad (10)$$

where  $m_l^p$  is the magnitude of each track and  $oz_l^p$ ,  $ox_l^p$ , and  $oy_l^p$  denote the cosine of the angle after projecting two consecutive adjacent point tracks in the  $z$ ,  $x$ , and  $y$  axes plus one, respectively. We rescale all features into the range of 0 to 10 for each feature to be comparable and to satisfy the non-negative constraint of the NMF formulation.

For further clustering, all the motion features are combined into a single  $5(L-1) \times P$  non-negative matrix  $\mathbf{U} = [\mathbf{u}_1, \dots, \mathbf{u}_n] \in \mathbb{R}_+^{m \times n}$ , where the  $p$ -th column is given by

$$\mathbf{u}_p = [m_1^p, \dots, m_{L-1}^p, oz_1^p, \dots, oz_{L-1}^p, ox_1^p, \dots, ox_{L-1}^p, oy_1^p, \dots, oy_{L-1}^p]^T.$$

Since each value of the features is non-negative, they can be input to our framework.

### D. Graph-regularized Sparse NMF

1) *NMF*: Using a non-negative feature matrix  $\mathbf{U}$  built by the motion quantities described above and  $k \leq \min(m, n)$ , let  $\mathbf{V} = [v_{ik}] \in \mathbb{R}_+^{m \times k}$  be the *building blocks* and  $\mathbf{W} = [w_{kj}] \in \mathbb{R}_+^{k \times n}$  be the *weighting map*, respectively. The objective of NMF is to produce two output non-negative matrices (i.e.,  $\mathbf{U} \approx \mathbf{V}\mathbf{W}$ ): (1) spatial building blocks, which can change over time and (2) a weighting map of those blocks, which weights them over time. We define NMF using the Frobenius norm to minimize the reconstruction error between  $\mathbf{U}$  and  $\mathbf{V}\mathbf{W}$  [1] as given by

$$\mathcal{E}(\mathbf{V}, \mathbf{W}) = \|\mathbf{U} - \mathbf{V}\mathbf{W}\|_F^2 = \sum_{i,j} \left( u_{ij} - \sum_{k=1}^K v_{ik} w_{kj} \right)^2 \quad (11)$$

where  $\|\cdot\|_F$  is the matrix Frobenius norm. A popular choice to solve this is to use the multiplicative update rule [1]:

$$\mathbf{V} \leftarrow \mathbf{V} * \mathbf{U}\mathbf{W}^T ./ \mathbf{V}\mathbf{W}\mathbf{W}^T \quad (12)$$

$$\mathbf{W} \leftarrow \mathbf{W} * \mathbf{V}^T \mathbf{U} ./ \mathbf{V}^T \mathbf{V}\mathbf{W} \quad (13)$$

2) *Sparsity Constraint*: Once we obtain the building blocks and weighting map, the weighting map is used to identify the cohesive region, which in turn exhibits functional units. Since there could be many possible weighting maps to generate the same movements, a sparsity constraint is incorporated into the weighting map so that the obtained functional units represent optimized and simplest tongue behaviors to generate target movements. This is also analogous with the current wisdom on phonological theories [18]. In essence, we use the sparsity constraint to encode the high-dimensional and complex tongue motion data using a small set of active (or non-negative) components so that the obtained weighting map is simple and easy to interpret. Within the sparse NMF framework, it has been reported that a fractional regularizer using the  $L_{1/2}$  norm provided superior performance to the  $L_1$  norm regularization by producing sparser solutions [38]. Thus, in this work, we use the  $L_{1/2}$  sparsity constraint in our NMF framework, which is given by

$$\mathcal{E}(\mathbf{V}, \mathbf{W}) = \frac{1}{2} \|\mathbf{U} - \mathbf{V}\mathbf{W}\|_F^2 + \eta \|\mathbf{W}\|_{1/2}. \quad (14)$$

Here, the parameter  $\eta \geq 0$  is a weight associated with the sparseness of  $\mathbf{W}$  and  $\|\mathbf{W}\|_{1/2}$  is expressed as

$$\|\mathbf{W}\|_{1/2} = \left( \sum_{i=1}^k \sum_{j=1}^n w_{ij}^{1/2} \right)^2. \quad (15)$$

3) *Manifold Regularization*: Despite the high-dimensional configuration space of human motions, many motions lie on low-dimensional and non-Euclidean manifolds [37]. NMF with the sparsity constraint described above, however, produces a weighting map using a Euclidean structure in the high-dimensional space. Therefore, the intrinsic and geometric relation between motion quantities cannot be captured faithfully in the sparse NMF formulation. Thus, we added a manifold regularization to capture the intrinsic geometric structure similar to [23], [39], [40]. The manifold regularization additionally preserves the local geometric structure. Our final cost function using both the regularizations is then given by

$$\mathcal{E}(\mathbf{V}, \mathbf{W}) = \frac{1}{2} \|\mathbf{U} - \mathbf{V}\mathbf{W}\|_F^2 + \frac{1}{2} \lambda \text{Tr}(\mathbf{W}\mathbf{L}\mathbf{W}^T) + \eta \|\mathbf{W}\|_{1/2} \quad (16)$$

where  $\lambda$  is a weight associated with the manifold regularization,  $\text{Tr}(\cdot)$  is the trace of a matrix,  $\mathbf{Q}$  is a heat kernel weighting,  $\mathbf{D}$  is a diagonal matrix, where  $D_{jj} = \sum_l Q_{jl}$ , and  $\mathbf{L} = \mathbf{D} - \mathbf{Q}$ , which is the graph Laplacian.

4) *Minimization*: Due to the non-convex cost function in Eq. (16), a multiplicative iterative method is adopted akin to that used in [40]. Let  $\Psi = [\psi_{mk}]$  and  $\Phi = [\phi_{kn}]$  be Lagrange multipliers subject to  $v_{mk} \geq 0$  and  $w_{kn} \geq 0$ , respectively. We solve this using the Lagrangian by the definition of

the Frobenius norm,  $\|\mathbf{U}\|_F = (\text{Tr}(\mathbf{U}^T\mathbf{U}))^{1/2}$ , and matrix calculus given by

$$\begin{aligned} \mathcal{L} = & \frac{1}{2}\text{Tr}(\mathbf{U}\mathbf{U}^T) - \text{Tr}(\mathbf{U}\mathbf{W}^T\mathbf{V}^T) + \frac{1}{2}\text{Tr}(\mathbf{V}\mathbf{W}\mathbf{W}^T\mathbf{V}^T) \\ & + \frac{\lambda}{2}\text{Tr}(\mathbf{W}\mathbf{L}\mathbf{W}^T) + \text{Tr}(\mathbf{\Psi}\mathbf{V}^T) + \text{Tr}(\mathbf{\Phi}\mathbf{W}^T) + \eta\|\mathbf{W}\|_{1/2}. \end{aligned} \quad (17)$$

The partial derivatives of  $\mathcal{L}$  with respect to  $\mathbf{V}$  and  $\mathbf{W}$  are given by

$$\begin{aligned} \frac{\partial \mathcal{L}}{\partial \mathbf{V}} &= -\mathbf{U}\mathbf{W}^T + \mathbf{V}\mathbf{W}\mathbf{W}^T + \mathbf{\Psi} \\ \frac{\partial \mathcal{L}}{\partial \mathbf{W}} &= -\mathbf{V}^T\mathbf{U} + \mathbf{V}^T\mathbf{V}\mathbf{W} + \lambda\mathbf{W}\mathbf{L} + \frac{\eta}{2}\mathbf{W}^{-1/2} + \mathbf{\Phi}. \end{aligned} \quad (18)$$

Finally, the update rule is found by using Karush-Kuhn-Tucker conditions—i.e.,  $\mathbf{\Psi}_{mk}\mathbf{V}_{mk} = 0$  and  $\mathbf{\Phi}_{kn}\mathbf{W}_{kn} = 0$ :

$$\begin{aligned} \mathbf{V} &\leftarrow \mathbf{V} * \mathbf{U}\mathbf{W}^T ./ \mathbf{V}\mathbf{W}\mathbf{W}^T \\ \mathbf{W} &\leftarrow \mathbf{W} * (\mathbf{V}^T\mathbf{U} + \lambda\mathbf{W}\mathbf{Q}) ./ (\mathbf{V}^T\mathbf{V}\mathbf{W} + \frac{\eta}{2}\mathbf{W}^{-1/2} + \lambda\mathbf{W}\mathbf{D}). \end{aligned} \quad (19)$$

### E. Spectral Clustering

Now that we obtain the building blocks and their associated weighting map in Eq. (19), spectral clustering is applied to the weighting map which represents a measure of tissue point similarity. It has been reported that spectral clustering outperforms conventional clustering methods such as the K-means algorithm [41]. Therefore, we use spectral clustering to obtain the final clustering results, which in turn reveals the cohesive motion patterns.

More specifically, from the weighting map  $\mathbf{W}$  as in Eq. (19), an affinity matrix  $\mathbf{A}$  is constructed:

$$\mathbf{A}(i, j) = \exp\left(-\frac{\|w(i) - w(j)\|_2}{\sigma}\right), \quad (20)$$

where  $w(i)$  represents the  $i$ -th column vector of  $\mathbf{W}$  and  $\sigma$  is the scale. In our experiment, we chose  $\sigma = 0.01$ . Within the graph cut framework, nodes in the graph is formed by the column vectors of  $\mathbf{W}$ , and the edge weights indicates the similarity  $\mathbf{A}$  computed between column vectors of  $\mathbf{W}$ . On the affinity matrix, we apply spectral clustering using a normalized cut algorithm [42]. From a graph cut point of view, our method can be seen as identifying sub-graphs representing characteristic motions that are different from one another.

### F. Model Selection

To achieve the best clustering quality, we need to select the optimal number  $k$  of clusters, which however is a challenging task [45]. In this work, we build a consensus matrix whose entries represent probabilities that samples  $i$  and  $j$  belong to the same cluster by repeating NMF 10 times. Then, the dispersion coefficient  $\rho$  of a consensus matrix  $C$  is defined as

$$\rho = \frac{1}{n^2} \sum_{i=1}^m \sum_{j=1}^n 4(\tilde{c}_{ij} - 0.5)^2, \quad (21)$$

where  $\tilde{c}_{ij}$ ,  $m$ , and  $n$  denote each entry of the matrix, the row and column size of the matrix, respectively. In the ideal case,

for a consensus matrix whose entries are all 0s or 1s, we have  $\rho = 1$ ; for a scattered consensus matrix, we have  $0 < \rho < 1$ . The optimal number of clusters is determined as the one with the maximal  $\rho_k$  [46]. We set  $2 \leq k \leq 6$  in this work.

TABLE I  
CLUSTERING PERFORMANCE: NMI AND AC

NMI (%)	K-means	N-Cut	GS-NMF-K	Our method
COIL20 ( $\mathcal{K}=20$ )	73.80%	76.56%	90.11%	<b>90.63%</b>
PIE ( $\mathcal{K}=68$ )	54.40%	77.13%	89.95%	<b>91.74%</b>
Tongue ( $\mathcal{K}=7$ )	96.99%	99.25%	97.50%	<b>99.69%</b>
Tongue ( $\mathcal{K}=8$ )	97.77%	99.61%	98.51%	<b>99.67%</b>
AC (%)	K-means	N-Cut	GS-NMF-K	Our method
COIL20 ( $\mathcal{K}=20$ )	60.48%	66.52%	83.75%	<b>85.00%</b>
PIE ( $\mathcal{K}=68$ )	23.91%	65.91%	79.93%	<b>84.31%</b>
Tongue ( $\mathcal{K}=7$ )	98.41%	99.71%	98.51%	<b>99.90%</b>
Tongue ( $\mathcal{K}=8$ )	98.72%	99.85%	99.14%	<b>99.88%</b>

## IV. EXPERIMENTAL RESULTS

In this section, we describe the qualitative and quantitative evaluation to validate the proposed method. We use 2D image and tongue data, and 3D simulated tongue motion data to demonstrate the accuracy of our approach. Furthermore, 3D *in vivo* human tongue motion datasets are used to identify functional units during protrusion and simple speech tasks.

### A. Experiments Using 2D Image and Synthetic Motion Data

We used three 2D datasets to validate our method. The first two datasets include the COIL20 image database and the CMU PIE database, each having 20 classes and 68 classes, respectively. As our third dataset, we used 2D synthetic tongue motion data containing a displacement field from two time frames as shown in Figure 2, where we tested 7 and 8 classes. Our method was compared against K-means clustering, a normalized cut method (N-Cut) [42], and graph-regularized sparse NMF with K-means clustering (GS-NMF-K) [23]. To measure the accuracy, two measures including the Normalized Mutual Information (NMI) and the clustering accuracy (AC) were used similar to [23]. Table 1 lists the two measures, showing that our method outperforms other methods. In addition, the  $L_{1/2}$  and  $L_1$  norms were compared experimentally, demonstrating that the  $L_{1/2}$  norm performed better.

### B. Experiments Using 3D Synthetic Tongue Motion Data

We also assessed the performance of the proposed method using four synthetic tongue motion datasets, since there is no ground truth in our tongue motion data. We used a composite Lagrangian displacement field of individual muscle groups based on a tongue atlas [11]. Each muscle group was defined by a mask volume with a value of 1 inside the muscle group, and zero elsewhere. Since the masks were known, it also provided ground truth labels to examine the accuracy of the output of our method. The first and second datasets used genioglossus (GG) and superior longitudinal (SL) muscles with and without interdigitated regions. The GG muscle was translated while the SL muscle was rotated  $-0.1$  radians about the  $x$  direction in Fig. 3(A) in the course of 11 time

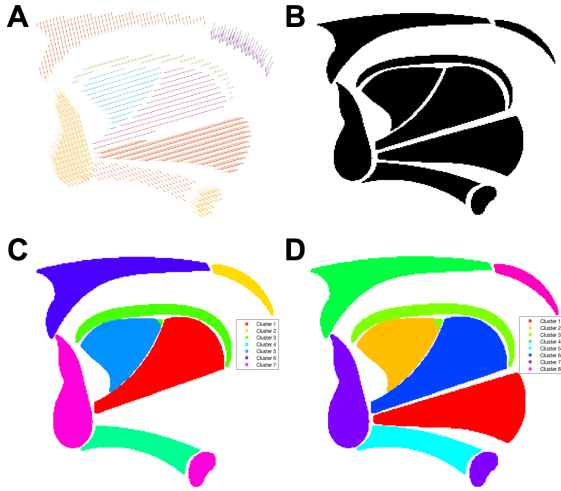


Fig. 2. Illustration of 2D synthetic tongue motion simulation results: (A) a quiver plot of the synthetic displacement field for each region ( $K=8$ ), (B) ground truth labels ( $K=8$ ), (C) clustering results of 7 regions using our method, and (D) clustering results of 8 regions using our method.

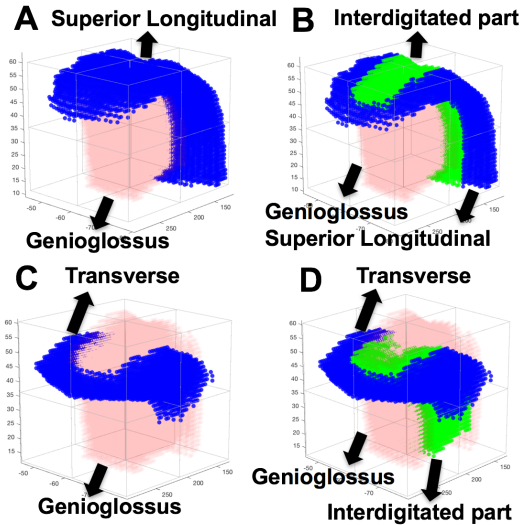


Fig. 3. Illustration of clustering results for 3D synthetic tongue motion simulations: (A) translation plus rotation without interdigitated regions (2 clusters), (B) rotations with interdigitated regions (3 clusters), (C) translation plus rotation without interdigitated regions (2 clusters), and (D) rotations with interdigitated regions (3 clusters). It is noted that our approach identified each label accurately as visually assessed.

frames. The GG muscle was rotated  $-0.1$  radians about the  $x$  direction while the SL muscle was rotated  $0.1$  radians about the  $x$  direction in Fig. 3(B) in the course of 11 time frames. The third and fourth datasets were generated by applying the same composite Lagrangian displacement field to the GG and transverse muscles with and without interdigitated regions as in Fig. 3(C) and (D), respectively. Fig. 3 showed the final clustering results using our method. We attempted to cluster each dataset into two (first and third datasets) and three (second and fourth datasets) distinct motions, respectively, where we obtained 100% clustering accuracy for all datasets when evaluated against the ground truth labels.

### C. Experiments Using 3D In Vivo Tongue Motion Data

TABLE II  
CHARACTERISTICS OF *in vivo* TONGUE MOTION DATA

Task	Protrusion	/s/-/u/	/i/-/s/
Time frames	1-13	10-17	15-22
Number of clusters	2-4	2-4	2-4

3D *in vivo* tongue motion data including protrusion and simple speech tasks such as “a souk” and “a geese” were used to identify functional units. One subject performed the protrusion task synchronized with metronome sound, and ten subjects performed “a souk” and “a geese” tasks using the same protocol. We used the same motion quantities described above as our input to the NMF framework. Table II lists the characteristics of our *in vivo* tongue motion data including time frames analyzed and the number of clusters extracted based on the dispersion coefficient.

First, we identified the functional units from the protrusion task, where Fig. 4 shows (B) two clusters, (C) three clusters, and (D) four clusters, respectively, based on the dispersion coefficient as depicted in Fig. 5 and visual assessment. The protrusion motion is characterized by forward and upward motion of the tongue as depicted in Fig. 4(A). Fig. 4(B) shows forward protrusion (red) vs. small motion (blue). In addition, as the number of clusters increases as shown in Fig. 4(C) and (D), subdivision of large regions in small motion (blue, Fig. 4(B)) into small functional units was observed.

Second, we identified the functional units during /s/ to /u/ from “a souk.” Fig. 6 depicts (B) two clusters, (C) three clusters, and (D) four clusters, respectively in the same manner. During the course of these motions, the tongue tip moves forward to upward/backward, while the tongue body and the posterior tongue move upward and forward, respectively as depicted in Fig. 6(A). Fig. 6(B) shows two clusters including the tip plus bottom of the tongue (red) vs. the tongue body. Three clusters in Fig. 6(C) show a good representation of the tip, body and posterior of the tongue and four clusters in Fig. 6(D) further subdivided the tongue tip and bottom.

Third, in the same manner, we identified the functional units during /i/ to /s/ from “a geese.” Fig. 8 displays (B) two clusters, (C) three clusters, and (D) four clusters, respectively. During the course of these motions, the tongue tip moves upward, while the tongue body moves backward and the posterior tongue moves forward as shown in Fig. 8(A). Two clusters in Fig. 8(B) show a division between the tip plus bottom of the tongue (red) and the tongue body. Three clusters in Fig. 8(C) are a good representation of the tip, body and posterior of the tongue and four clusters as depicted in Fig. 8(D) subdivided the posterior of the tongue further.

## V. DISCUSSION

In this work, we presented an approach for characterizing tongue’s multiple functional degrees of freedom, which is critical to understand the tongue’s role in speech and other lingual behaviors. This is because the functioning of the tongue in speech or other lingual behaviors entails successful orchestration of the complex system of 3D tongue muscular structures

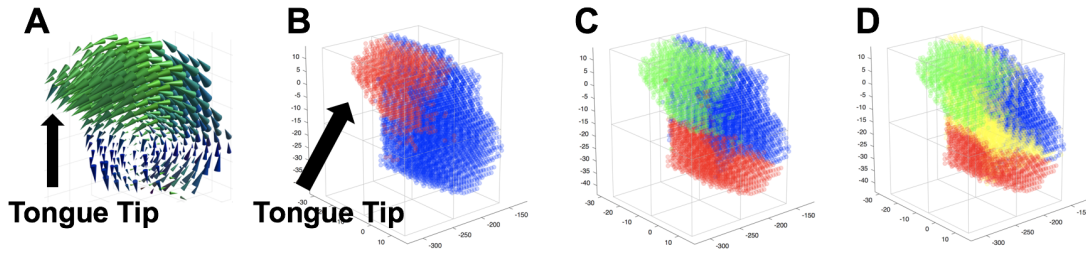


Fig. 4. Illustration of identified functional units using our method during the tongue protrusion task, depicting (A) 3D Lagrangian displacement field, (B) final functional units (2 clusters), (C) final functional units (3 clusters), and (D) final functional units (4 clusters). Please note that the displacement fields and clustering results are plotted relative to the first time frame representing the neutral tongue position.

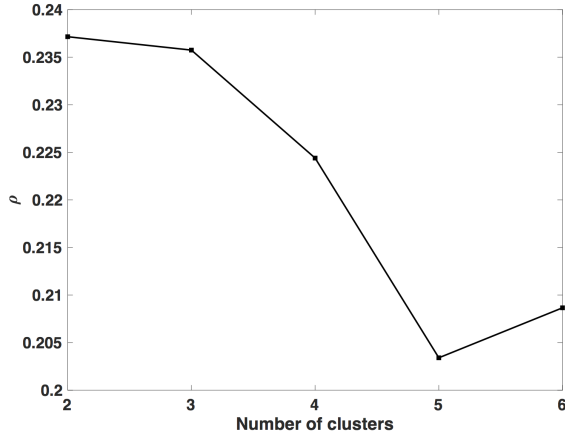


Fig. 5. Plot of the dispersion coefficient vs. the different number of clusters for the tongue protrusion task. Please note that we analyzed 2-4 clusters in our experiments.

over time. Determining functional units from healthy controls plays an important role in understanding motor control strategy, which in turn could elucidate pathological or adapted motor control strategy when analyzing patient data such as tongue cancer or Amyotrophic Lateral Sclerosis patients. It has been a long-sought problem that many researchers attempted using various techniques.

Utilizing recent advances in tMRI-based motion tracking and data mining schemes, a new method for identifying functional units from MRI was presented, which opens new windows for a better understanding of the underlying tongue behaviors and for studying speech production. Unsupervised data clustering using sparse NMF is the task of identifying semantically meaningful clusters using a low-dimensional representation from a dataset. Different from previous algorithms, our proposed work aimed at identifying physiologically meaningful and coherent manifold structures of high-dimensional tongue motion data. Two constraints in addition to the standard NMF were employed to reflect the physiological properties of 4D tongue motion during protrusion and simple speech tasks. Firstly, the sparsity constraint was introduced to capture the simplest and the most optimized weighting map. Sparsity has been one of important properties for phonological theories [18], and our work attempted to decode this phenomenon within a sparse NMF framework. Secondly, the manifold regularization was added to capture the intrinsic and geometric

relationship between motion features. It also allows preserving the geometric structure between motion features, which is particularly important when dealing with tongue motions that lie on low-dimensional non-Euclidean manifolds.

In the experiments using 3D tongue motion simulation data, the testing motions in Fig. 3(A) and (C) included rotations about the styloid process and displacements about the inferosuperior directions, which is consistent with *in vivo* tongue movements. As for the input features, we used the magnitude and angle of point tracks derived from tMRI. More features could be investigated such as those reflect mechanical properties including principal strains, curvature, minimum-jerk, or two-thirds power law [48] or motion descriptors combining those individual features.

The number of clusters is often determined manually as there is no definite model selection method available. In this work, we built a “consensus matrix” from multiple runs for each  $k$  and assessed the presence of block structure. As an alternative, one can compare reconstruction errors for different number  $k$  or examine the stability (i.e., an agreement between results) from multiple randomly initialized runs for each  $k$ . Because there is no ground truth in our tongue data, we have used both visual assessment and the model selection approach in which the model selection approach provided an upper limit of the number of clusters.

There are a few directions to improve the current work. First, we used a data-driven approach to determine the functional units, which was visually assessed because of the lack of ground truth. This could be improved by further studies using model-based approaches via biomechanical stimulations [43] or electromyography [44] to co-validate our findings. For biomechanical simulations, subject-specific anatomy and the associated weighting map could be input and inverse simulation can then be used to verify the validity of the obtained weighting map. Second, we used the magnitude and orientation of point tracks as our input features. In order to equal the weight of each input feature, we normalized the feature values in the same range. In our future work, we will further study automatic relevance determination methods to model the interactions among these features to yield the best clustering outcome. Finally, the identified functional units as shown in our experimental results may involve multiple regions that correspond to sub-muscle or multiple muscles. Therefore, we will further study the identified functional units in the context of the muscular anatomy from individual high-resolution MRI,

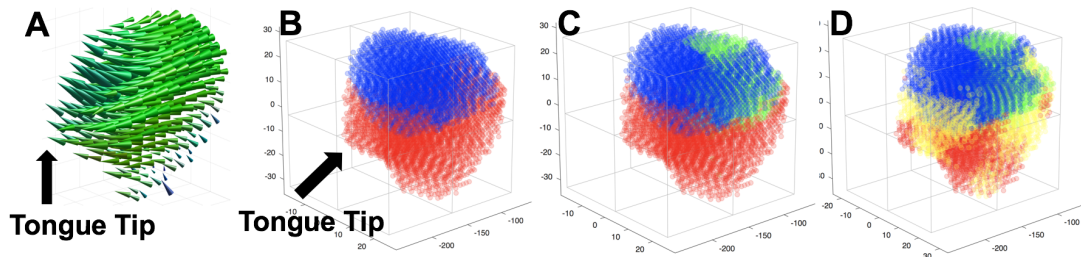


Fig. 6. Illustration of identified functional units using our method during /s/ to /u/ from “a souk,” depicting (A) 3D Lagrangian displacement field, (B) final functional units (2 clusters), (C) final functional units (3 clusters), and (D) final functional units (4 clusters). Please note that the displacement fields and clustering results are plotted relative to the first time frame representing the neutral tongue position.

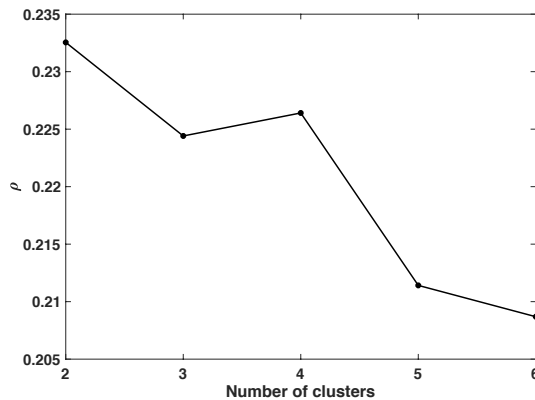


Fig. 7. Plot of the dispersion coefficient vs. the different number of clusters for the task of /s/ to /u/ from “a souk.” Please note that we analyzed 2-4 clusters in our experiments.

diffusion MRI, or a vocal tract atlas [11].

## VI. CONCLUSION

We have presented a new algorithm to determine local functional units that link muscle activity to surface tongue geometry during protrusion and simple speech tasks. We evaluated the performance of our approach using various simulated and human tongue motion datasets, demonstrating that our method surpassed conventional methods and accurately clustered the human tongue motion. Our results suggest that it is feasible to identify the functional units using a set of motion features, which has great potential in the improvement of diagnosis, treatment, and rehabilitation in patients with speech-related disorders.

## ACKNOWLEDGMENT

This research was in part supported by NIH R21DC016047, R00DC012575, R01DC014717, and R01CA133015.

## REFERENCES

- [1] D. D. Lee, H. S. Seung, “Learning the parts of objects by non-negative matrix factorization,” *Nature*, 401(6755), pp. 788–791, 1999
- [2] G. Trigeorgis, K. Bousmalis, S. Zafeiriou, B. W. Schuller, “A deep matrix factorization method for learning attribute representations,” *IEEE Trans. Pattern Analysis and Machine Intelligence*, 39(3), 417–429, 2017
- [3] M. Stone, M. A. Epstein, K. Iskarous, “Functional segments in tongue movement,” *Clinical Linguistics & Phonetics*, 18(6-8), pp. 507–21, 2004
- [4] J. R. O’Kusky and M. G. Norman, “Sudden infant death syndrome: increased number of synapses in the hypoglossal nucleus,” *Journal of Neuropathology and Experimental Neurology*, 54, pp. 627–34, 1995
- [5] V. Parthasarathy, J. L. Prince, M. Stone, E. Z. Murano, M. NessAiver, “Measuring tongue motion from tagged cine-MRI using harmonic phase (HARP) processing,” *Journal of the Acoustical Society of America*, 121(1), pp. 491–504, January, 2007
- [6] J. R. Green, “Tongue-surface movement patterns during speech and swallowing,” *The Journal of the Acoustical Society of America*, 113(5), pp. 2820–33, 2003
- [7] J. A. S. Kelso, “Synergies: Atoms of Brain and Behavior,” *In Progress in Motor Control*, pp. 83–91, Springer, 2009
- [8] M. Stone, E. P. Davis, A. S. Douglas, M. N. Aiver, R. Gullapalli, W. S. Levine, A. J. Lundberg, “Tongue-surface movement patterns during speech and swallowing,” *Journal of Speech, Language, and Hearing Research*, 113(5), pp. 2820–2833, 2001
- [9] E. Bresch, Y. C. Kim, K. Nayak, D. Byrd, S. Narayanan, “Seeing speech: Capturing vocal tract shaping using real-time magnetic resonance imaging,” *IEEE Signal Processing Magazine*, 25(3), pp. 123–132, 2008
- [10] M. Fu, Z. Bo, C. Carignan, R. K. Shosted, J. L. Perry, D. P. Kuehn, Z.P. Liang, and B. P. Sutton, “High-resolution dynamic speech imaging with joint lowrank and sparsity constraints,” *Magnetic Resonance in Medicine*, 73(5), pp. 1820–32, 2015
- [11] J. Woo, J. Lee, E. Murano, F. Xing, A. Meena, M. Stone and J. Prince, “A high-resolution atlas and statistical model of the vocal tract from structural MRI,” *Computer Methods in Biomechanics and Biomedical Engineering: Imaging & Visualization*, pp. 1–14, 2015
- [12] M. Stone, J. Woo, J. Lee, T. Poole, A. Seagraves, M. Chung, E. Kim, E. Z. Murano, J. L. Prince, S. S. Blemker, “Structure and variability in human tongue muscle anatomy,” *Computer Methods in Biomechanics and Biomedical Engineering: Imaging & Visualization*, pp. 1–9, 2016
- [13] F. Xing, J. Woo, E. Z. Murano, J. Lee, M. Stone, J. L. Prince, “3D tongue motion from tagged and cine MR images,” *International Conference on Medical Image Computing and Computer Assisted Intervention (MICCAI)*, LNCS 8151, pp. 41–48, 2013
- [14] B. Gick and I. Stavness, “Modularizing speech,” *Frontiers in psychology*, 4, pp. 1–3, 2013
- [15] M. Stone, “A three-dimensional model of tongue movement based on ultrasound and x-ray microbeam data,” *Journal of the Acoustical Society of America*, 87, pp. 2207–17, 1990
- [16] V. Ramanarayanan, L. Goldstein, and S. Narayanan, “Spatio-temporal articulatory movement primitives during speech production: extraction, interpretation, and validation,” *Journal of the Acoustical Society of America*, 134(2), pp. 1378–1394, 2013
- [17] J. Woo, F. Xing, J. Lee, M. Stone, J. L. Prince, “Determining Functional Units of Tongue Motion via Graph-regularized Sparse Non-negative Matrix Factorization,” *International Conference on Medical Image Computing and Computer Assisted Intervention (MICCAI)*, 17(Pt 2), pp. 146–53, 2014
- [18] C. Browman and L. Goldstein, “Dynamics and articulatory phonology,” in *Mind as Motion: Explorations in the Dynamics of Cognition*, edited by R. F. Port and T.van Gelder (MIT Press, Cambridge, MA), pp. 175–194, 1995
- [19] T. Li and C. H. Q. Ding, “Nonnegative Matrix Factorizations for Clustering: A Survey,” In: *Data Clustering: Algorithms and Applications*. Chapman and Hall/CRC, pp. 149–176, 2013
- [20] N. F. Osman, W. S. Kerwin, E. R. McVeigh, J. L. Prince, “Cardiac motion tracking using CINE harmonic phase (HARP) magnetic resonance imaging,” *Magnetic resonance in medicine*, 42(6), pp. 1048–60, 1999

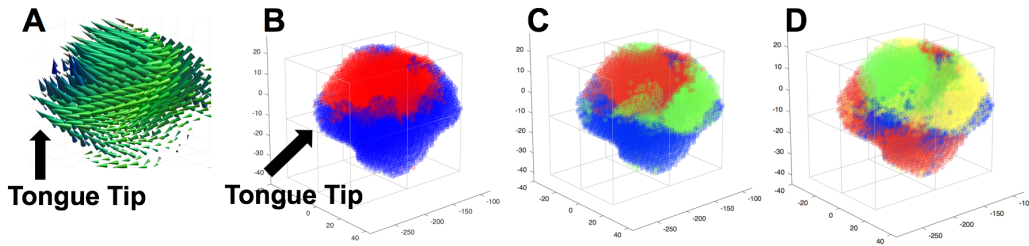


Fig. 8. Illustration of identified functional units using our method during /i/ to /s/ from “a geese,” depicting (A) 3D Lagrangian displacement field, (B) final functional units (2 clusters), (C) final functional units (3 clusters), and (D) final functional units (4 clusters). Please note that the displacement fields and clustering results are plotted relative to the first time frame representing the neutral tongue position.

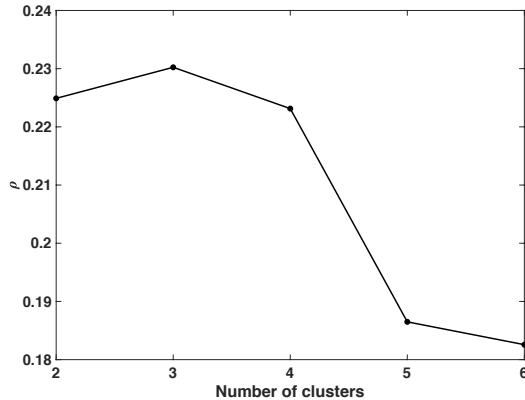


Fig. 9. Plot of the dispersion coefficient vs. the different number of clusters for the task of /i/ to /s/ from “a geese.” Please note that we analyzed 2-4 clusters in our experiments.

- [21] T. Mansi, X. Pennec, M. Sermesant, H. Delingette, and N. Ayache, “iLogDemons: A demons-based registration algorithm for tracking incompressible elastic biological tissues,” *International journal of computer vision*, 92(1), pp. 92–111, 2011
- [22] F. Xing, C. Ye, J. Woo, M. Stone, J. L. Prince, “Relating speech production to tongue muscle compressions using tagged and high-resolution magnetic resonance imaging,” *SPIE Medical Imaging*, Florida, FL, 2015
- [23] D. Cai, X. He, J. Han, T. S. Huang, “Graph regularized nonnegative matrix factorization for data representation,” *IEEE Trans. Pattern Analysis and Machine Intelligence*, 33(8), pp. 1548–1560, 2011
- [24] H. Shinagawa, E. Z. Murano, J. Zhuo, B. Landman, R. Gullapalli, and J. L. Prince, M. Stone, “Tongue muscle fiber tracking during rest and tongue protrusion with oral appliances: A preliminary study with diffusion tensor imaging,” *Acoustical science and technology*, 29(4), pp. 291–294, 2008
- [25] T. A. Gaige, T. Benner, R. Wang, V. J. Wedeen, R. J. Gilbert, R.J., “Three dimensional myoarchitecture of the human tongue determined in vivo by diffusion tensor imaging with tractography,” *Journal of Magnetic Resonance Imaging*, 26(3), pp. 654–661, 2007
- [26] M. NessAiver and J. L. Prince, “Magnitude image CSPAMM reconstruction (MICSr),” *Magnetic Resonance in Medicine*, 50(2), pp. 331–342, 2003
- [27] J. Woo, M. Stone, Y. Suo, E. Murano, J. L. Prince, “Tissue-Point Motion Tracking in the Tongue From Cine MRI and Tagged MRI,” *Journal of Speech, Language, and Hearing Research*, 57(2), pp. 626–636, 2013
- [28] J. Kim and H. Park, “Sparse nonnegative matrix factorization for clustering,” Technical Report GT-CSE-08-01, Georgia Institute of Technology, 2008
- [29] F. Shahnaz, M. W. Berry, V. P. Pauca, and R. J. Plemmons, “Document clustering using nonnegative matrix factorization,” *Information Processing and Management*, 42(2), pp. 373–386, 2006
- [30] Y. Gao, G. Church, “Improving molecular cancer class discovery through sparse non-negative matrix factorization,” *Bioinformatics*, 21(21), pp. 3970–3975, 2005
- [31] J. Wang, X. Wang, X. Gao, “Non-negative matrix factorization by maximizing correntropy for cancer clustering,” *BMC Bioinformatics*, 14(1), pp. 1–11, 2013
- [32] A. Anderson, P. K. Douglas, W. T. Kerr, V. S. Haynes, A. L. Yuille, A.L., J. Xie, Y. N. Wu, J. A. Brown, M. S. Cohen, “Non-negative matrix factorization of multimodal MRI, fMRI and phenotypic data reveals differential changes in default mode subnetworks in ADHD,” *NeuroImage*, 102(1), pp. 207–219, 2014
- [33] Q. Mo, and B. A. Draper, “Semi-nonnegative matrix factorization for motion segmentation with missing data,” *European Conference on Computer Vision*, pp. 402–415, Berlin, Heidelberg, 2012
- [34] A. Cheriyyadat and R. J. Radke, “Non-negative matrix factorization of partial track data for motion segmentation,” *IEEE 12th International Conference in Computer Vision*, pp. 865–872, 2009
- [35] F. Xing, J. Woo, A. Gomez, D. L. Pham, P. V. Bayly, M. Stone, and J. L. Prince, “Phase Vector Incompressible Registration Algorithm (PVIRA) for Motion Estimation from Tagged Magnetic Resonance Images,” *IEEE Trans on Medical Imaging*, 36(10), pp. 2116–2128, Oct, 2017
- [36] F. Xing, J. Woo, E. Z. Murano, J. Lee, M. Stone, J. L. Prince, “3D tongue motion from tagged and cine MR images,” 16th International Conference on Medical Image Computing and Computer Assisted Intervention (MIC-CAI), Nagoya, Japan, pp. 865–872, Sep, 2013
- [37] A. Elgammal and C. S. Lee, “The role of manifold learning in human motion analysis,” In B. Rosenhahn, R. Klette, D. Metaxas, (eds.) *Human Motion. Computational Imaging and Vision*, 36, pp. 25–56, 2008
- [38] Y. Qian, S. Jia, J. Zhou, J., A. Robles-Kelly, “Hyperspectral unmixing via sparsity-constrained nonnegative matrix factorization,” *IEEE Transactions on Geoscience and Remote Sensing*, pp. 4282–4297, 2011
- [39] S. Yang, C. Hou, C. Zhang, Y. Wu, “Hyperspectral unmixing via sparsity-constrained nonnegative matrix factorization,” *IEEE Transactions on Geoscience and Remote Sensing*, pp. 4282–4297, 2011
- [40] X. Lu, H. Wu, Y. Yuan, P. Yan, X. Li, “Manifold regularized sparse NMF for hyperspectral unmixing,” *IEEE Transactions on Geoscience and Remote Sensing*, 51(5), pp. 2815–26, 2013
- [41] U. Von Luxburg, “A tutorial on spectral clustering,” *Statistics and Computing*, 17(4), pp. 395–416, 2007
- [42] J. Shi and J. Malik, “Normalized cuts and image segmentation,” *IEEE Transactions on Pattern Analysis and Machine Intelligence*, 22(8), pp. 888–905, 2000
- [43] I. Stavness, J. E. Lloyd and S. Fels, “Automatic prediction of tongue muscle activations using a finite element model,” *Journal of Biomechanics*, 45(16), pp. 2841–2848, 2012
- [44] L. Pittman and E. F. Bailey, “Genioglossus and intrinsic electromyographic activities in impeded and unimpeded protrusion tasks,” *Journal of Neurophysiology*, 101(1), pp. 276–282, 2009
- [45] Z. Zhang, Y., T. Li., C. Ding, R., X.-W., and X. S. Zhang, “Binary matrix factorization for analyzing gene expression data. *Data Mining and Knowledge Discovery*,” 20(1), pp. 28–52, 2010
- [46] K. Da, J. Choo, and H. Park, “Nonnegative matrix factorization for interactive topic modeling and document clustering,” In *Partitional Clustering Algorithms*, pp. 215–243, 2015
- [47] C. Boutsidis and E. Gallopoulos, “SVD based initialization: A head start for nonnegative matrix factorization,” *Pattern Recognition*, 41(4), pp. 1350-1362, 2008
- [48] P. Viviani, T. Flash, “Minimum-jerk, two-thirds power law, and isochrony: converging approaches to movement planning,” *Journal of Experimental Psychology: Human Perception and Performance*, 21(1), pp. 32–53, 1995
- [49] J. Woo, F. Xing, M. Stone, J. Green, T. Reese, T. Brady, V. Wedeen, J. Prince, and G. El Fakhri, “Speech Map: A Statistical Multimodal Atlas of 4D Tongue Motion During Speech from Tagged and Cine MR Images,” *Journal of Computer Methods in Biomechanics and Biomedical Engineering (CMBBE): Special Issue on Imaging and Visualization*, 2017